Electron Momentum Spectroscopy of 1-Butene: A Theoretical Analysis Using Molecular Dynamics and Molecular Quantum Similarity

ARTICLE *in* THE JOURNAL OF PHYSICAL CHEMISTRY A · JULY 2013

Impact Factor: 2.69 · DOI: 10.1021/jp405122p · Source: PubMed

4 AUTHORS, INCLUDING:

Seiyed Hamid Reza Shojaei
Hasselt University
10 PUBLICATIONS **30** CITATIONS

SEE PROFILE

Michael S Deleuze
Hasselt University
132 PUBLICATIONS **2,672** CITATIONS

SEE PROFILE

THE JOURNAL OF PHYSICAL CHEMISTRY A

Article

pubs.acs.org/JPCA

Electron Momentum Spectroscopy of 1-Butene: A Theoretical Analysis Using Molecular Dynamics and Molecular Quantum Similarity

S. H. Reza Shojaei,[†] Jelle Vandenbussche,[‡] Michael S. Deleuze,*[,†] and Patrick Bultinck[‡]

[†]Research Group of Theoretical Chemistry and Molecular Modelling, Hasselt University, Agoralaan, Gebouw D, B-3590 Diepenbeek, Belgium

[‡]Department of Inorganic and Physical Chemistry, Ghent University, Krijgslaan 281 (S3), B9000 Ghent, Belgium

ABSTRACT: The results of experimental studies of the valence electronic structure of 1-butene by means of electron momentum spectroscopy (EMS) have been reinterpreted on the basis of molecular dynamical simulations in conjunction with the classical MM3 force field. The computed atomic trajectories demonstrate the importance of thermally induced nuclear dynamics in the electronic neutral ground state, in the form of significant deviations from stationary points on the potential energy surface and considerable variations of the C−C−C−C dihedral angle. These motions are found to have a considerable influence on the computed spectral bands and outer-valence electron momentum distributions. Euclidean distances between spherically averaged electron momentum densities confirm that thermally induced nuclear motions need to be fully taken into account for a consistent interpretation of the results of EMS experiments on conformationally flexible molecules.

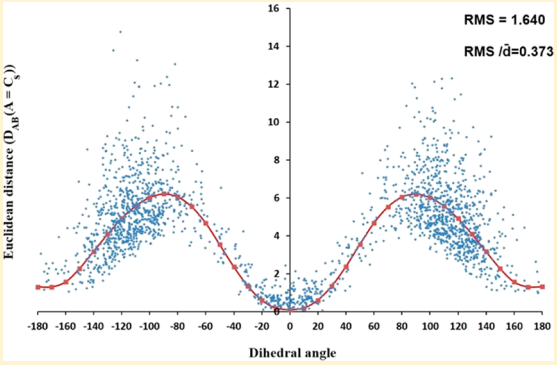

INTRODUCTION

1-Butene is the simplest alkene able to possess conformational isomers due to hindered rotations about the middle C−C bond. Indications of the existence of two almost isoenergetic conformers have been found[1−9] over many years in spectroscopies of various types, including infrared, Raman, nuclear magnetic resonance, microwave, and femtosecond nonlinear spectroscopies. These structures, of C_s and C_1 symmetry, are characterized by C−C−C−C dihedral angles (τ) of 0° and about ±120° and are most commonly referred to as the cis (synplanar, or more simply syn) and gauche conformers, respectively. The energy minima corresponding to these structures are separated by rather sizable energy barriers, of the order of ∼1.8 and ∼1.2 kcal mol^{-1}, relating to the so-called skin ($\tau \approx 180°$) and skew ($\tau \approx 60°$) transition states, respectively. The most recent theoretical estimates, of CCSD(T) [coupled cluster theory with single, double, and perturbative triple excitations] quality in conjunction with an asymptotically complete basis set, indicate an energy difference of 0.025 kcal mol^{-1} only (8.72 cm^{-1}) in favor of the gauche (C_1) conformer.[10] In a recent study[11,12] of the molecular and electronic structure of 1-butene employing electron momentum spectroscopy (EMS),[13−17] a powerful experimental orbital-imaging technique, a (significantly much larger) Gibb's free energy difference of 0.47 ± 0.20 kcal mol^{-1} (164 ± 70 cm^{-1}) was deduced in favor of the gauche form from the experimentally obtained conformational weights.

With this spectroscopic approach, spherically averaged orbital momentum distributions are inferred from an angular analysis of ionization intensities obtained in coincidence at specific electron binding energies (ε_b) from (e,2e) electron impact ionization experiments ($M + e^- [E_0 + \varepsilon_b] \rightarrow M^+ + 2e^- [E_0/2]$) at high kinetic energies (typically, with E_0 in the range 1.2−2.4 keV), using a noncoplanar symmetric kinematic setup for maximizing the momentum transfer and ensuring therefore a clean "knock-out" (e,2e) process. Since a pioneering study on *n*-butane,[18] the archetype of conformationally flexible molecules, it is well-established[19−25] that conformational rearrangements may leave strong fingerprints, throughout the inner- and outer-valence regions, in the electron momentum distributions that can be experimentally obtained from EMS experiments for specific orbitals or sets of orbitals. The influence of the molecular conformation on the computed momentum distributions is often strong enough to justify the idea of using EMS for evaluating conformational abundances and conformer energy differences, assuming thermal equilibrium between energy minima. A weakness of this depiction, however, is that it does not account for the fact that thermally induced nuclear motions may result into substantial deviations from equilibrium structures corresponding to energy minima on the potential energy surface. In a recent study on tetrahydrofuran,[26] we have unraveled the outcome in EMS experiments of internal pseudorotational motions and of their coupling with further internal degrees of freedom, by resorting to the principles of

Received: May 24, 2013
Revised: July 30, 2013
Published: July 31, 2013

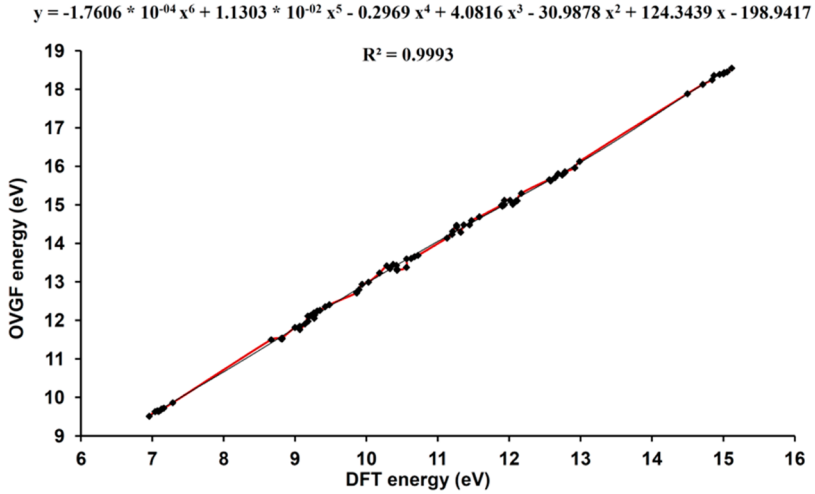

Figure 1. Correlation between OVGF/aug-cc-pVTZ ionization and B3LYP/aug-cc-pVTZ occupied orbital energies. All energy values are in eV.

simulations employing molecular dynamics (MD).[27] The main advantage of this approach is that, by virtue of the ergodic principle, it enables a complete exploration of the phase space, which is equivalent to an ensemble average over all internal degrees of freedom, such as is computed in Monte Carlo simulations. MD simulations therefore directly account for entropy effects, and complications such as hindered rotations.

In the present work, we wish to also employ the principles of MD simulations for reinterpreting the results of the EMS studies by Chen et al.[11,12] of the valence electronic structure of 1-butene. The main motivation to this work stems from the observation that, in spite of all efforts made so far for coping with complications such as hindered rotations by means of statistical thermodynamics and modeling electron momentum distributions as accurately as possible using benchmark Dyson orbitals,[28] large discrepancies with experiment remain in the latest theoretical study of these results.[10] We also put forward the hypothesis that these discrepancies may be the consequence of considering only contributions from the minimum energy structures on the potential energy surface, thus excluding most thermally induced structural variations. MD may obviously be used to address this issue and to investigate the extent of structural deviations from energy minima as well as their influence on electron momentum distributions. However, EMS spectroscopy relies on momentum densities and these are not so trivially linked to structural variation as position and momentum spaces are quite different. Using the principles of so-called molecular quantum similarity,[29] we therefore computed for all structures in the MD run geometrical distances in spherically averaged momentum densities with respect to the minima on the potential energy surface. Applications of molecular quantum similarity in momentum space are relatively few with respect to position space, but have been shown to reflect different similarities compared to position space.[30−33] Given the already mentioned relationship between EMS spectroscopy and momentum space, momentum space based similarity can shed light on the importance of the suspected effects of thermally induced nuclear motions in the electronic neutral ground state. As will be shown from the quantum similarity data, thermally induced deviations from the minimum energy structures need to be fully taken into account for consistent insights into the experimentally obtained (e,2e) electron momentum profiles.

THEORY AND COMPUTATIONAL DETAILS

All MD calculations presented in this work have been performed using the 4.2 version of the TINKER package of programs[34] in conjunction with the classical MM3 force field,[35−37] which has been especially designed for computing conformational energies and rotational barriers in cyclic and cage compounds.[38−40] Compared with the results of temperature-dependent nuclear magnetic resonance (NMR) measurements, this force field was found to yield consistent insights into complex molecular motions, such as the circumrotations of benzylic amide catenanes.[41] The accuracy of the MM3 force field has been also verified in a detailed study of the torsional characteristics of *trans*-stilbene and comparison with benchmark quantum mechanical data.[42] A temperature of 298 K has been used in the MD//MM3 simulations through coupling of the system with an external bath using the Groningen method.[43] The atom trajectories have been calculated using the modified Beeman algorithm,[44] along with the following inputs for the MD computations: an integration time step of 1 fs along with punching of nuclear coordinates at every 10 ps, for a total run time of 20 ns, resulting in the generation of 2000 essentially independent and properly thermalized structures. The initial structure used in these simulations was inferred from combined ab initio predictions and microwave data.[4]

All molecular structures produced by the MD//MM3 simulations were used as input geometries in single point calculations employing density functional theory (DFT) along with the Becke-3-parameters-Lee−Yang−Parr (B3LYP) functional[45,46] or the dispersion corrected ωB97XD exchange-correlation functional[47] and Dunning's augmented correlation consistent polarized valence basis set of double-ζ quality (aug-cc-pVDZ).[48,49] Homemade C-shell scripts have been developed to automatically convert the molecular coordinates output of the MD//MM3 runs into input for B3LYP/aug-cc-pVDZ and ωB97XD/aug-cc-pVDZ calculations of the electronic wave function, using the Gaussian 09 package of programs,[50] and to combine results for further analysis. Specifically, the results of these B3LYP/aug-cc-pVDZ and ωB97XD/aug-cc-pVDZ calculations were used in turn to compute thermally averaged ionization spectra and (e,2e) electron momentum distributions.

For a consistent analysis of electron momentum distributions of conformationally flexible molecules inferred from the angular dependence of (e,2e) ionization cross sections at specific

dx.doi.org/10.1021/jp405122p | J. Phys. Chem. A 2013, 117, 8388−8398

ionization energies, it is essential[18,20] to account for the influence of the molecular conformation on the energy order and relative distribution of ionization lines, and determine in particular to which ionization band each ionization line contributes. Given the computational cost of accurate one-electron ionization energies, especially for a large number of structures without any particular symmetry, we opted to obtain one-electron ionization energies of OVGF[51,52] (outer valence Green's function) quality from Kohn−Sham B3LYP/aug-cc-pVTZ occupied orbital energies. For 10 randomly chosen structures produced in the course of the MD//MM3 simulations, the Kohn−Sham B3LYP/aug-cc-pVTZ occupied orbital energies were computed and compared with OVGF/aug-cc-pVTZ valence one-electron ionization energies. The following regression equation was found to optimally reproduce the latter ionization energies (y) from the Kohn−Sham B3LYP/aug-cc-pVTZ occupied orbital energies (x):

$$y = -1.7606 \times 10^{-4}x^6 + 0.0113x^5 - 0.2969x^4 + 4.0816x^3 - 30.9878x^2 + 124.3439x - 198.9417 \quad (1)$$

This equation shows that the linear term has clearly the largest coefficient and indeed, a simple linear regression between both sets of energies leads to $R^2 = 0.9989$. Nevertheless, in what follows, the above sixth-order regression is used for all practical purposes as it has a still slightly higher regression coefficient ($R^2 = 0.9993$) and allows avoiding the need for massive numbers of OVGF calculations. Although a standard view expressed in the literature[53] is that Kohn−Sham orbital energies have no definite physical meaning, an extension of Koopmans's theorem to DFT demonstrates that these energies represent approximations to relaxed ionization energies.[54] The fact that the proposed regression between B3LYP/aug-cc-pVTZ Kohn−Sham orbitals energies and OVGF/aug-cc-pVDZ ionization energies is almost linear (Figure 1) is in line with the view[55] that there exist simple scaling relationships between Kohn−Sham orbital energies and ionization energies.

Another sixth-order regression equation ($R^2 = 0.9993$) similar to eq 1 was used to obtain one-electron ionization energies of OVGF/aug-cc-pVTZ quality (y) from Kohn−Sham ωB97XD/aug-cc-pVTZ orbital energies (x).

$$y = -1.3676 \times 10^{-4}x^6 + 0.0106x^5 - 0.3401x^4 + 5.7254x^3 - 53.5527x^2 + 265.1119x - 536.7154 \quad (2)$$

OVGF pole strengths were found to be larger than 0.85 at binding energies ranging from 9 to 19 eV, indicating[56−58] that, in the investigated energy range, the one-electron picture of ionization[59] prevails. According to CCSD(T)/aug-cc-pVTZ results, the vertical double ionization energy thresholds of the gauche and cis conformers of 1-butene are located at ∼26.9 and 27.0 eV, respectively. Shake-off bands are therefore unlikely to play any role in the investigated binding energy range.

Theoretical ionization spectra have been constructed by convoluting the rescaled B3LYP/aug-cc-pVTZ occupied orbital energies, assuming that all ionization lines have the same spectroscopic strength ($\Gamma = 1$) and using as convolution function a Voigt profile combining a Gaussian and a Lorentzian function with equal weight and a constant full width at half-maximum (fwhm) parameter of 0.2 or 0.8 eV. These parameters have been chosen to allow meaningful comparisons with available ultraviolet He I photoelectron or EMS measurements, respectively, taking into account the corresponding experimental resolution as well as the average natural line width. We note that the vibrational contribution to band broadening is accounted for by virtue of the MD//MM3 simulations.

Spherically averaged orbital momentum distributions have been generated for each resolved ionization band from single point B3LYP/aug-cc-pVDZ and ωB97XD/aug-cc-pVDZ calculations, using the MOMAP program by Brion and co-workers,[60] and homemade interfaces. The B3LYP exchange-correlation functional was selected, because it is known to yield spherically averaged electron momentum distributions approaching the results of benchmark Dyson orbital calculations.[61,62] In order to enable physically meaningful comparisons with the latest experimental momentum profiles by Chen et al.,[11] the theoretical spherically averaged momentum distributions have been convoluted with the experimental momentum resolution, using Monte Carlo methods,[63] and according to an experimental angular resolution of 0.84° and 0.57° on azimuthal and polar angles, respectively. The theoretical electron momentum distributions have been recast onto the relative intensity scales defined by the (e,2e) experimental electron counts measured by Chen et al. in their EMS study of 1-butene,[11] using a global rescaling factor obtained from a least-squares fit between the experimental and theoretical (e,2e) ionization intensities for all valence ionization lines, up to electron binding energies of 18.69 eV.

Lacking the original numerical data, experimental (e,2e) ionization cross sections were obtained by digitizing the experimental momentum distributions presented in ref 11, as a function of the target electron momentum, by means of the so-called "GetData Graph Digitizer" package.[64]

The dependence of (e,2e) momentum distributions associated to specific ionization bands onto the molecular conformation and further thermal distortions (bond stretchings, angle bendings, etc.) of the molecular structure is quantified by means of Euclidean distances that were computed between spherically averaged electron momentum densities (SAEMDs), according to the following definitions:

$$D_{AB} = \sqrt{Z_{AA} + Z_{BB} - 2Z_{AB}} \quad (3)$$

$$Z_{AB} = \int_0^\infty \pi_A^0(p)\pi_B^0(p)\, dp \quad (4)$$

In the above equations, A and B denote specifically two different conformations of the target molecule (1-butene) for which the relevant SAEMDs are represented as $\pi_A^0(p)$ and $\pi_B^0(p)$. The latter are obtained from the Fourier transforms of partial one-electron density matrices corresponding to the Kohn−Sham orbitals that contribute to the ionization band of interest

$$\rho_A(\mathbf{r}, \mathbf{r}') = \sum_{i\in\alpha} \phi_i^*(\mathbf{r})\phi_i(\mathbf{r}') \quad (5)$$

where α represents the set of (Kohn−Sham) orbitals that possess an estimated ionization energy in the required electron binding energy range (see the Results and Discussion section for numerical details), according to the sixth order regression of eq 1.

The Fourier transformation of the density matrix in eq 5 yields

dx.doi.org/10.1021/jp405122p | J. Phys. Chem. A 2013, 117, 8388−8398

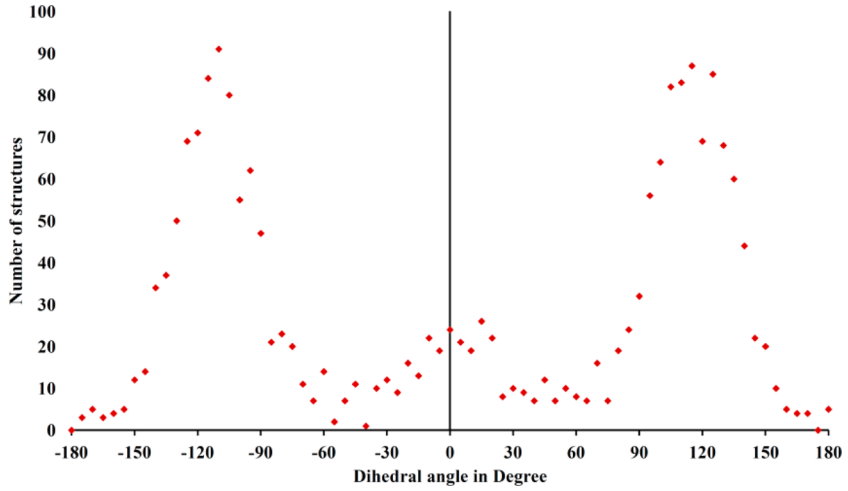

Figure 2. Distribution of the molecular structures dumped from the MD//MM3 trajectories as a function of the internal C−C−C−C dihedral angle (step size of 5°).

$$\pi_A(\mathbf{p}, \mathbf{p}') = (2\pi)^{-3} \int d\mathbf{r}\, d\mathbf{r}' \rho_A(\mathbf{r}, \mathbf{r}') e^{-i(\mathbf{p}\cdot\mathbf{r}-\mathbf{p}'\cdot\mathbf{r}')} \quad (6)$$

This implies using Fourier transformation of the basis, after which the momentum density is obtained by setting $\mathbf{p} = \mathbf{p}'$ in eq 6 followed by spherical averaging:

$$\pi_A^0(p) = \frac{1}{4\pi} \int_0^{2\pi} \int_0^{\pi} \pi_A(\mathbf{p}, \mathbf{p}) \sin(\theta)\, d\theta\, d\phi \quad (7)$$

As is clear from the above, our method implies the Fourier transformation of (partial) one-electron density matrices obtained from Kohn−Sham orbitals. These are, however, based on a system of noninteracting electrons and even if the exact functional would be known, there is no guarantee that the (total) one-electron density in momentum space would also be exact.[65] The momentum density from Kohn−Sham DFT has been compared to one-electron momentum densities obtained from (post-)Hartree−Fock computations, showing that for the limited set of functionals tested, DFT does not per se perform better than Hartree−Fock theory.[66,67] On the other hand, Ragot argued that DFT momentum densities are not per se worse than Hartree−Fock ones.[68] For the sake of consistency with our analysis of (e,2e) momentum distributions, we chose to compute Euclidean distances between (partial) B3LYP/aug-cc-pVDZ Kohn−Sham momentum densities. In EMS, (e,2e) ionization cross sections relate to structure factors obtained as the square of the Fourier Transform to momentum space of Dyson orbitals,[13] to which Hartree−Fock orbitals are poor approximations. Indeed, compared with the results of EMS experiments, Hartree−Fock orbitals rather often lead severe underestimations of orbital momentum densities at low electron momenta (see, e.g., ref 61). In contrast, Kohn−Sham orbitals are known to be suitable approximations to Dyson orbitals[69] and have been widely used therefore for interpreting EMS experiments.

Since the employed momentum profiles in eq 4 are spherically averaged and electron momentum densities (EMDs) are monocentric distributions with a common origin (unlike their position space counterparts), an additional step involving the structural alignment of A and B is conveniently avoided. The integrals (eq 4) were evaluated numerically using Laguerre quadrature for a polynomial order of 250. Spherical averaging was performed using confluent hypergeometric functions, as outlined in ref 70.

We note that the index Z_{AB} obtained from eq 3 provides an effective measure of momentum-space quantum similarity between structures A and B. Because eq 3 is consistent with

$$D_{AB}^2 = \int_0^{\infty} dp\, [\pi_A^0(p) - \pi_B^0(p)]^2 \quad (8)$$

it follows that D_{AB} satisfies all requirements associated with a true distance measure:

$$D_{AB} \in \mathbf{R}_0^+ \quad (9)$$

$$D_{AA} = 0 \quad (10)$$

$$D_{AB} = D_{BA} \quad (11)$$

$$D_{AB} \leq D_{AC} + D_{CB} \quad (12)$$

D_{AB} identically vanishes in case of a perfect match between $\pi_A^0(p)$ and $\pi_B^0(p)$. The more these two momentum-space density functions differ, the smaller will be the value of the quantum similarity index Z_{AB}, and the larger will be the value of the Euclidian distance D_{AB}. In the forthcoming discussion, we will consider Euclidean distances computed at the B3LYP/aug-cc-pVDZ level by comparing the SAEMDs of all structures dumped from the MD//MM3 trajectories with the SAEMDs of the cis (C_s) and gauche (C_1) energy minimum forms, for the purpose of quantifying the global effect of thermally induced nuclear motions on these momentum distributions. In order to more specifically evaluate the effect of changes of the molecular conformation on the computed SAEMDs, comparison will be made with Euclidean distances obtained with respect to the cis and gauche energy minima from structures obtained by systematically varying the C−C−C−C dihedral angle (τ) in steps of 10° from −180° to +180°, and by reoptimizing subsequently at the B3LYP/aug-cc-pVTZ level all other structural parameters. For the sake of conciseness in the analysis, this second subset of (37) structures will in the following be referred to as the "model conformational ensemble" (MCE), whereas the set of (2000) structures dumped from the MD//MM3 trajectories will be referred to as the "model thermal ensemble" (MTE).

dx.doi.org/10.1021/jp405122p | J. Phys. Chem. A 2013, 117, 8388−8398

RESULTS AND DISCUSSION

Prior to deciphering the ionization spectra and electron momentum distributions of 1-butene on MD grounds, it is useful to note first that MM3 results enable us to investigate the conformational energy differences of 1-butene at a level of accuracy approaching that of a CCSD(T)/aug-cc-pVDZ treatment. In line with benchmark theoretical data,[10] both approaches describe the gauche (C_1) conformer as being the most stable one. The MM3 force field locates the cis (C_s) conformer, the skin, and the skew transition state structures at 0.38, 2.23, and 5.29 kcal mol^{-1} above the gauche conformer, respectively. At the CCSD(T)/aug-cc-pVDZ level of theory, the cis (C_s) conformer, the skin, and the skew transition states are located correspondingly at 0.26, 2.04, and 4.62 kcal mol^{-1} above the gauche conformer. The accuracy of the MM3 force field is therefore sufficient for the purpose of generating reliable enough conformer distributions from molecular dynamical simulations, coping explicitly with further complications like entropy effects and hindered rotations.

The reader is referred to Figure 2 for a distribution of all molecular structures dumped from the MD//MM3 simulations defining our model thermal ensemble (MTE) as a function of the internal C−C−C−C dihedral angle (τ). In line with their lower energy, gauche structures are found to dominate the ensemble at room temperature. The widths of the peaks around ($\tau \approx 0°$) and ($|\tau| \approx 120°$) in the histogram of Figure 2 demonstrate nevertheless the importance of thermally induced nuclear dynamics in the neutral electronic ground state, in the form of significant deviations of numerous structures extracted from the MD atomic trajectories from the structure of the cis and gauche energy minimum forms. Such deviations must therefore be taken into account for a sufficiently consistent discussion of the influence of the temperature on the ionization spectra and electron momentum distributions of 1-butene.

In Figure 3 and Table 1, we compare the He I ultraviolet photoelectron spectrum of 1-butene recorded by White et al. (Figure 3a)[71] with convoluted densities of states that are the results (Figure 3b) of calculations based on MD//MM3 simulations and thermal averaging therefore over 2000 structures, using B3LYP/aug-cc-pVTZ orbital energies that were rescaled according to eq 1. In spite of the neglect of photoionization cross sections, the main features of the experimental spectrum are correctly reproduced by our simulations, within an overall accuracy of 0.4 eV on the location of bands, which is in line with the standard expectation for a calculation of OVGF quality.

The (e,2e) ionization spectrum recorded by Chen et al.[11] at an azimuthal angle (ϕ) of 9° is compared in Figure 4 with the results of the MD//MM3 simulations, in conjunction with B3LYP/aug-cc-pVTZ single-point calculations of rescaled orbital energies (eq 1) and of the electron momentum densities measuring at this azimuthal angle the relative (e,2e) ionization intensites of each occupied orbital. The experimental (e,2e) ionization spectrum is displayed along with (Figure 4a) the six Gaussian bands used by Chen et al.[11] for convoluting their EMS measurements. We correspondingly display in Figure 5 the theoretically predicted (e,2e) ionization spectrum of 1-butene, obtained after integrating the momentum-energy density map on ϕ, starting from 0° to 10° in steps of 2°. Our MD//MM3 simulations (Figure 4b, Figure 5) indicate at first glance that at electron binding energies ranging from 8 to 20 eV, the EMS measurements by Chen et al. for 1-butene can

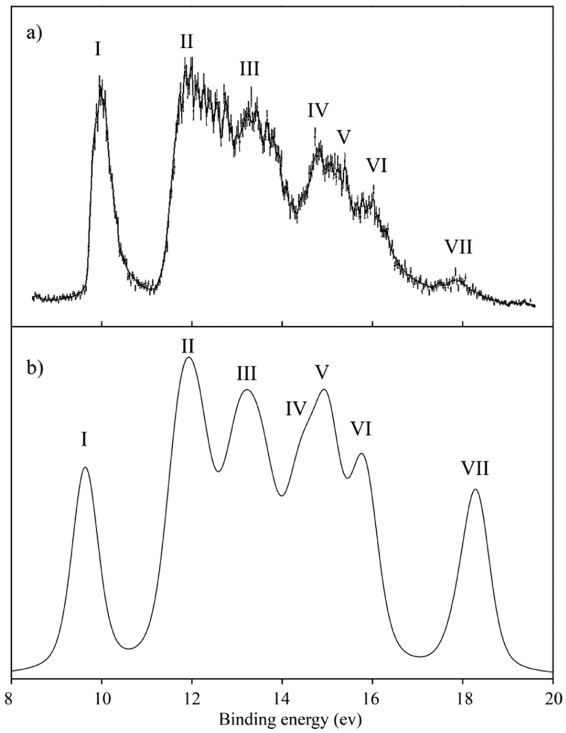

Figure 3. Comparison of the (a) He I photoelectron spectrum of 1-butene by White et al.,[71] with (b) thermally averaged MD//MM3 simulations of OVGF/aug-cc-pVTZ quality (see text for explanation, fwhm = 0.2 eV).

Table 1. Comparison of Theoretical OVGF Ionization Spectra with Experimental Data[a]

level	theoretical UPS[b]	He I (21.22 eV)[c]	theoretical EMS[b]	experimental EMS (E_0 = 1200 eV)[d]
1	I (9.6)	I (9.9)	A (9.64)	A (10.0)
2	II (11.9)	II (12.0)	B (12.04)	B (12.0)
3	III (13.2)	III (13.4)	C (13.18)	C (13.4)
4	IV (14.5)	IV (14.8)	D (14.98)	D (14.8)
5	V (14.9)	V (15.4)		
6	VI (15.8)	VI (16.0)	E (15.68)	E (15.9)
7	VII (18.3)	VII (17.9)	F (18.28)	F (18.3)

[a]Electron binding energies are in eV. [b]This work. [c]see ref 71. [d]see ref 11.

be analyzed in terms of six ionization bands (A, B, C, D, E, and F). However, severe overlaps due to the limited energy resolution prevent meaningful experimental reconstructions of orbital momentum profiles from separate angular analyses of the (e,2e) ionization intensities characterizing bands B, C, D, and E. In line with the analysis by Chen et al.,[11] the experimental (e,2e) momentum profiles corresponding to the outer-valence energy region [8−20 eV] of 1-butene will therefore be interpreted in terms of four resolved ionization bands only (A, B+C, D+E, F), corresponding to ionization lines in the following electron binding energy ranges: 9.00 to 10.66 eV, 10.66 to 14.06 eV, 14.06 to 17.06 eV, and 17.06 to 19.00 eV, respectively. These energy ranges define the sets of orbitals (α) used in eqs 2−4 for computing quantum similarity indices and Euclidean distances between the SAEMDs associated to bands A, B+C, D+E, and F.

The experimental electron momentum profiles inferred by Chen et al.[11] from an angular analysis of the (e,2e) ionization

dx.doi.org/10.1021/jp405122p | J. Phys. Chem. A 2013, 117, 8388−8398

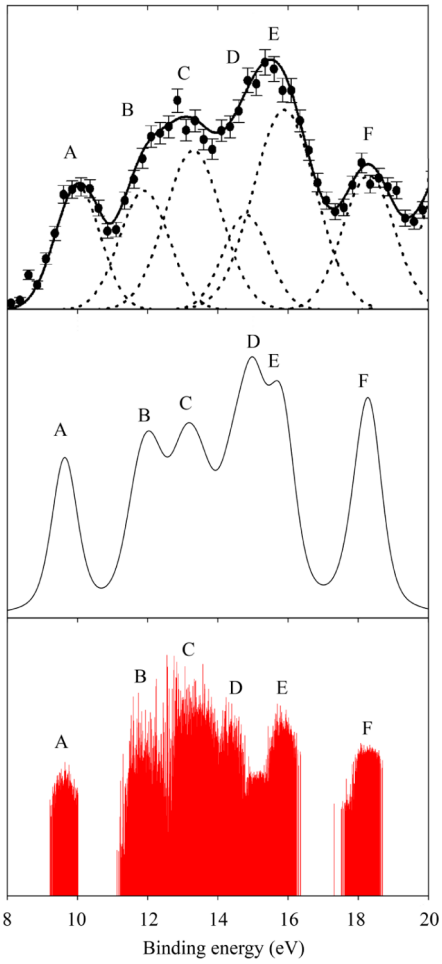

Figure 4. Experimental[11] and simulated (this work) binary (e,2e) ionization spectra of 1-butene at an azimuthal angle (ϕ) of 9°.

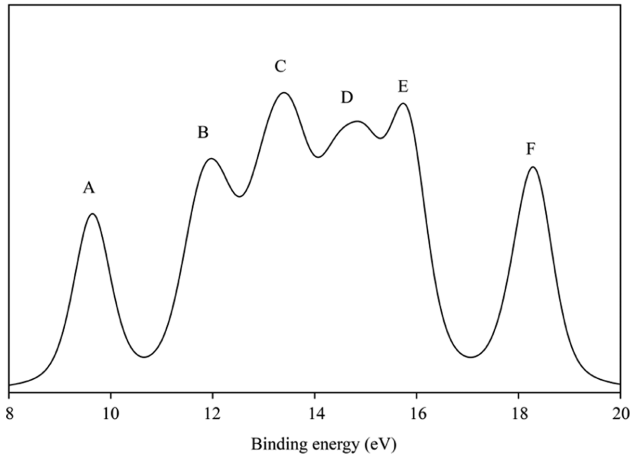

Figure 5. Simulation of the integrated (e,2e) ionization spectrum of 1-butene.

intensities characterizing these four ionization bands are compared in Figures 6a-9a with various theoretical simulations. These comprise the Dyson orbital ADC(3)/cc-pVDZ++ and Kohn−Sham orbital B3LYP/aug-cc-pVTZ momentum profiles obtained in ref 10 from a thermostatistical model assuming thermal equilibrium between the cis and gauche energy minimum forms, as well as thermally averaged B3LYP/aug-cc-pVDZ momentum profiles obtained from the model conformational ensemble (MCE), and thermally averaged B3LYP/aug-cc-pVDZ and ωB97XD/aug-cc-pVDZ momentum profiles obtained from the 2000 structures extracted from the MD//MM3 simulations, defining our model thermal ensemble

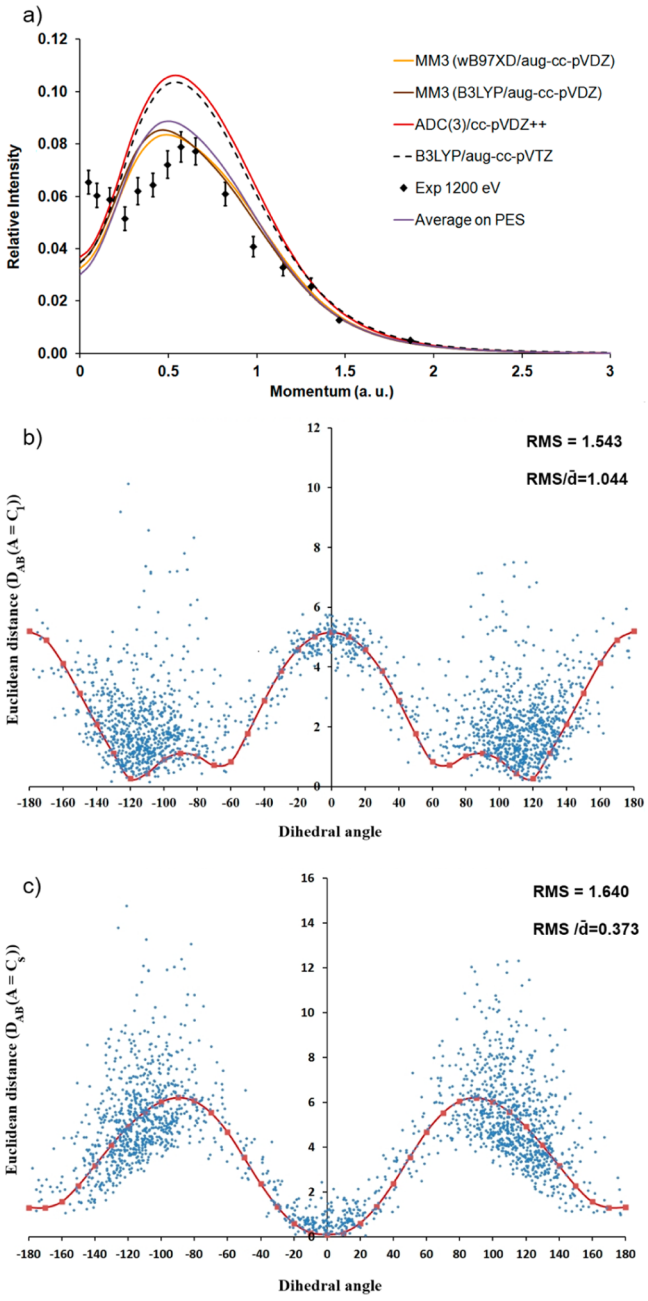

Figure 6. (a) Comparison between experimental and theoretical electron momentum distributions inferred at an electron impact energy of 1.2 keV (+ binding energy) for ionization lines at binding energies comprised between 9.00 and 10.64 eV (ionization band A); (b) analysis as a function of the C−C−C−C dihedral angle of the Euclidean distances between the SAEMDs obtained correspondingly from the model thermal ensemble (blue dots) and model conformational ensemble (red curve) with respect to the gauche (C_1) energy minimum form; (c) analysis as a function of the C−C−C−C dihedral angle of the Euclidean distances between the SAEMDs obtained correspondingly from the model thermal ensemble (blue dots) and model conformational ensemble (red curve) with respect to the cis (C_s) energy minimum form.

dx.doi.org/10.1021/jp405122p | J. Phys. Chem. A 2013, 117, 8388−8398

(MTE). We correspondingly display in Figures 6b−9b and 6c−9c plots of the Euclidean distances which were computed with respect to the gauche (C_1) and cis (C_s) energy minimum forms for all structures contributing to these model ensembles as a function of the C−C−C−C dihedral angle (τ). Upon

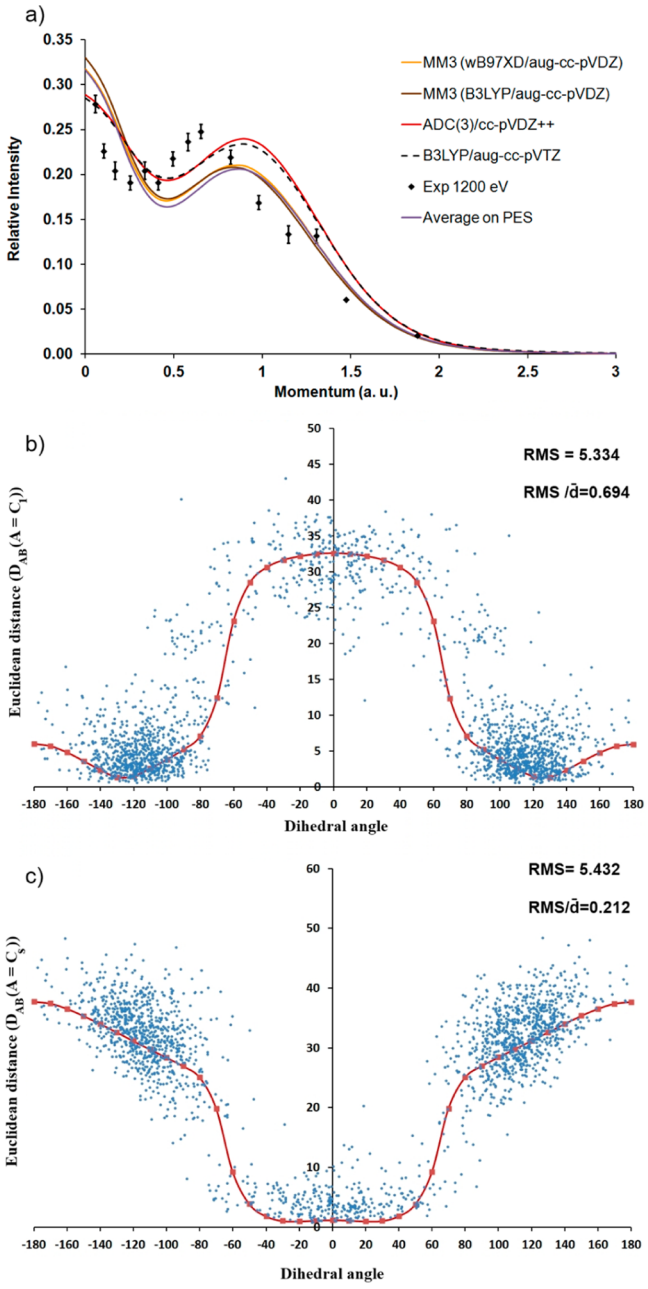

Figure 7. (a) Comparison between experimental and theoretical electron momentum distributions inferred at an electron impact energy of 1.2 keV (+ binding energy) for ionization lines at binding energies comprised between 10.64 and 14.06 eV (ionization bands B +C); (b) analysis as a function of the C−C−C−C dihedral angle of the Euclidean distances between the SAEMDs obtained correspondingly from the model thermal ensemble (blue dots) and model conformational ensemble (red curve) with respect to the gauche (C_1) energy minimum form; (c) analysis as a function of the C−C−C−C dihedral angle of the Euclidean distances between the SAEMDs obtained correspondingly from the model thermal ensemble (blue dots) and model conformational ensemble (red curve) with respect to the cis (C_s) energy minimum form.

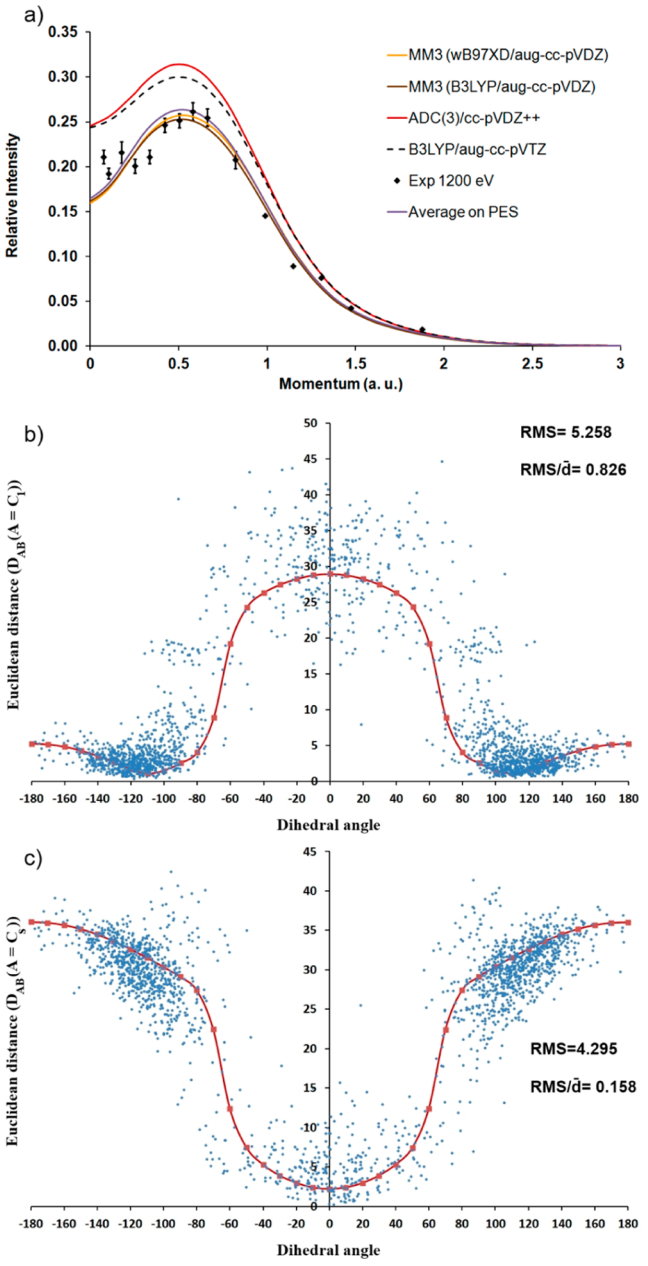

Figure 8. (a) Comparison between experimental and theoretical electron momentum distributions inferred at an electron impact energy of 1.2 keV (+ binding energy) for ionization lines at binding energies comprised between 14.06 and 17.06 eV (ionization bands D +E); (b) analysis as a function of the C−C−C−C dihedral angle of the Euclidean distances between the SAEMDs obtained correspondingly from the model thermal ensemble (blue dots) and model conformational ensemble (red curve) with respect to the gauche (C_1) energy minimum form; (c) analysis as a function of the C−C−C−C dihedral angle of the Euclidean distances between the SAEMDs obtained correspondingly from the model thermal ensemble (blue dots) and model conformational ensemble (red curve) with respect to the cis (C_s) energy minimum form.

examining Figures 6a−9a, it is clear that the ωB97XD/aug-cc-pVDZ and B3LYP/aug-cc-pVDZ electronic wave functions yield essentially the same thermally averaged and resolution folded SAEMDs. Also, thermally averaged and resolution folded SAEMDs obtained from the model thermal and conformational ensembles are very similar, indicating at first glance that the

dx.doi.org/10.1021/jp405122p | J. Phys. Chem. A 2013, 117, 8388−8398

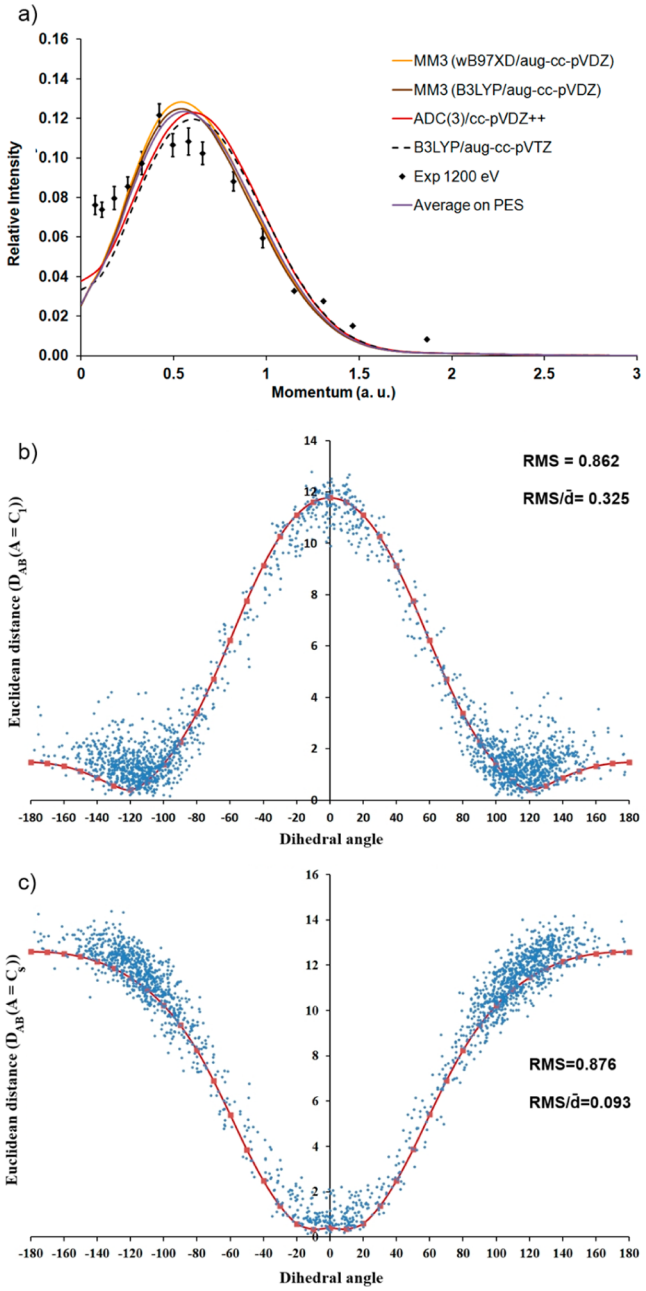

Figure 9. (a) Comparison between experimental and theoretical electron momentum distributions inferred at an electron impact energy of 1.2 keV (+ binding energy) for ionization lines at binding energies comprised between 17.06 and 19.00 eV (ionization band F); (b) analysis as a function of the C−C−C−-C dihedral angle of the Euclidean distances between the SAEMDs obtained correspondingly from the model thermal ensemble (blue dots) and model conformational ensemble (red curve) with respect to the gauche (C_1) energy minimum form; (c) analysis as a function of the C−C−C−C dihedral angle of the Euclidean distances between the SAEMDs obtained correspondingly from the model thermal ensemble (blue dots) and model conformational ensemble (red curve) with respect to the cis (C_s) energy minimum form.

molecular conformation is the factor that dictates the shape of the experimentally inferred electron momentum profiles. Compared with the results obtained previously[10] by considering the cis and gauche conformers only, accounting for thermally induced nuclear motions by averaging SAEMDs over the MTE and MCE enables us to reproduce more faithfully the experimental electron momentum profiles characterizing bands A and D+E (Figures 6a and 8a). For band F (Figure 9a), there is almost no difference. In contrast, a poorer agreement with experiment is observed for band B+C (Figure 7a).

Since the HOMO relates essentially to the π orbital associated with the double C═C bond, the corresponding momentum distribution (Figure 6a) is typically of the p-type. The MD//MM3 simulations for this energy level fail to reproduce a very strong turn-up of (e,2e) ionization intensities at electron momenta smaller than 0.25 au, which has been tentatively ascribed by Chen et al.[11] to distorted wave effects. In line with experiment, band (B+C) is found to produce a mixed s-p type momentum profile (Figure 7a), characterized by two maxima, among which one at p = 0 au. The MD//MM3 simulations indicate that bands (D+E) and F possess a p-type momentum profile (Figures 8a, 9a), characterized by one minimum at $p \approx 0$ au and one maximum at around $p \approx 0.5$ au . We note that for band F, all models so far fail to reproduce a significant turn-up in the experimental (e,2e) ionization intensities at $p < 0.25$ au.

Figures 6b−9b and 6c−9c show for each of the four identified ionization bands (A, B+C, D+E, and F) the Euclidean distances between the corresponding SAEMDs of every structure in the MTE and MCE on the one hand and those of the gauche (C_1) and cis (C_s) energy minima of 1-butene on the other. As was to be expected for quantum dissimilarity indices, these Euclidean distances sensitively reflect alterations of the molecular structure. Upon comparing from these figures results obtained from the MTE and MCE, it is clear that the molecular conformation is the factor that overall dominates the variability of the SAEMDs. Indeed, the distributions of Euclidean distances obtained from MTE rather faithfully follow the curves obtained from the MCE. In particular, with both sets of data, Euclidean distances with respect to the gauche (C_1) conformer (Figures 6b−9b) tend toward a minimum and a maximum when $\tau \approx \pm 120$ and $\tau \approx 0°$, respectively. In contrast, Euclidean distances with respect to the cis (C_s) conformer (Figures 6c−9c) tend toward a minimum and a maximum when $\tau \approx 0°$ and $\tau \approx \pm 90°$ (band A) or $\tau \approx \pm 180°$ (bands B +C, D+E, and F). Changes in the C−C−C−C dihedral angle and alterations of the molecular conformation alone do not explain the distribution of Euclidean distances which is obtained for the model thermal ensemble: these quantum dissimilarity indices also undoubtedly reflect further alterations of the molecular structure due to thermally induced nuclear motions, such as bond stretchings, angle bendings, methyl rotations, etc. Interestingly, Figures 6b−9b and 6c−9c also reveal another phenomenon. The root-mean-square differences (RMS) supplied in Figures 6b−9b and 6c−9c quantify the differences observed between the MTE (MD//MM3) and MCE sets of data. In these figures we also supply RMS data which were rescaled on the average MTE value ($\bar{d}$) obtained for the Euclidean distances. For a given value of the dihedral angle, the MTE and MCE SAEMD distances with either of the two minima may differ significantly. Recalling that in the MCE all geometric parameters except the dihedral angle are optimized, this shows that in the MD run there are also significant changes in the other geometrical parameters. These data therefore substantiate the observation that all internal degrees of freedom need to be taken into account for a complete and consistent analysis of the results of EMS experiments on a conformation-

dx.doi.org/10.1021/jp405122p | J. Phys. Chem. A 2013, 117, 8388−8398

ally flexible molecule. From these figures, and in line with the trends emerging from Figures 6a−9a, it is clear that the momentum profile for band A is the one most strongly affected by thermal effects beyond changes in the dihedral angle, which corroborates a high RMS/$\overline{d}$ index. In contrast, the very low RMS/$\overline{d}$ index computed for the momentum profile characterizing band F substantiates the extremely limited sensitivity of this profile to thermal effects. Bands B+C and D yield intermediate values for the RMS/$\overline{d}$ index, and the influence of thermal motions on the associated momentum profiles is therefore moderate.

CONCLUSIONS

In the present study, we have exploited the principles underlying molecular dynamical simulations for the purpose of unraveling the influence of thermally induced nuclear motions onto the ionization bands and (e,2e) electron momentum distributions of a conformationally flexible molecule: 1-butene. The results of experiments employing He I photoelectron spectroscopy as well as EMS on this compound have been reinterpreted on the basis of MD simulations in conjunction with the classical MM3 force field. An analysis of the structures dumped from the atomic trajectories demonstrates the importance of thermal deviations from stationary points on the potential energy surface, in the form of considerable variations of the C−C−C−C dihedral angle. These deviations are found to have a considerable influence on the computed spectral bands and outer-valence electron momentum distributions. Taking molecular dynamics into account enables us overall to more faithfully reproduce the experimentally inferred momentum distributions, with the exception of the momentum profile corresponding to the second ionization band (B+C) at ∼12 eV. The computation of Euclidean distances between the spherically averaged electron momentum densities characterizing the energy minimum structures and the structures extracted from the MD trajectories substantiates the conclusion that thermally induced nuclear motions involving all internal degrees of freedom in the electronic ground state need to be taken into account for a consistent interpretation of the results of EMS experiments on a conformationally flexible molecule. Indeed, the extreme variability in these quantum dissimilarity indices cannot be explained only by taking into account changes of the molecular conformation.

AUTHOR INFORMATION

Corresponding Author

*Tel: +32.11.26.83.03. E-mail: michael.deleuze@uhasselt.be.

Notes

The authors declare no competing financial interest.

ACKNOWLEDGMENTS

This work has been supported by the FWO_Vlaanderen, the Flemish branch of the Belgian National Science Foundation, and by the "Bijzonder OnderzoeksFonds" of Hasselt University. The authors especially acknowledge financial support within the framework of a Research Program of the Research Foundation-Flanders (FWO_Vlaanderen; Project No. G.0350.09N, entitled *From orbital imaging to quantum similarity in momentum space*).

REFERENCES

(1) Harrah, L. A.; Mayo, D. W. Rotational Isomerism Involving the 2−3 Carbon-Carbon Bond of the 1-Alkenes. *J. Chem. Phys.* **1960**, *33*, 298−299.
(2) Durig, J. R.; Compton, D. A. C. Spectroscopic and thermodynamic study of the conformational properties and torsional potential functions of 1-butene. *J. Phys. Chem.* **1980**, *84*, 773−781.
(3) Gallinella, E.; Cadioli, B. Infrared and Raman spectra, ab initio force field and vibrational assignment of the rotational isomers of 1-butene. *Vib. Spectrosc.* **1997**, *13*, 163−174.
(4) Bell, S.; Drew, B. R.; Guirgis, G. A.; Durig, J. R. The far infrared spectrum, ab initio calculations and conformational energy differences of 1-butene. *J. Mol. Struct.* **2000**, *553*, 199−219.
(5) Bothner-By, A. A.; Colin, C. N.; Gunther, H. The Proton Magnetic Resonance Spectra of Olefins. II. Internal Rotation in Alkylethylenes. *J. Am. Chem. Soc.* **1962**, *84*, 2748−2751.
(6) Karabatsos, G. J.; Taller, R. A. Structural studies by nuclear magnetic resonance-XIX: N,N-dimethylhydrazones and general comments on configurational and conformational isomerism. *Tetrahedron* **1968**, *24*, 3923−3937.
(7) Woller, P B; Garbisch, E W Conformational analysis of 1-butene. *J. Org. Chem.* **1972**, *37*, 4281−4285.
(8) Kondo, S.; Hirota, E.; Morino, Y. Microwave spectrum and rotational isomerism in butene-1. *J. Mol. Spectrosc.* **1968**, *28*, 471−489.
(9) Kunitski, M.; Knippenberg, S.; Dreuw, A.; Brutschy, B. The conformational stability of gaseous 1-butene studied by femtosecond nonlinear spectroscopy and ab initio calculations. *Vib. Spectrosc.* **2011**, *56*, 13−18.
(10) Shojaei, S. H. R.; Morini, F.; Hajgató, B.; Deleuze, M. S. Photoelectron and electron momentum spectroscopy of 1-butene at benchmark theoretical levels. *J. Phys. B* **2011**, *44*, 235101.
(11) Wu, F.; Chen, X. J.; Shan, X.; Tian, S. X.; Li, Z.; Xu, K. Conformational Stability of 1-Butene: An Electron Momentum Spectroscopy Investigation. *J. Phys. Chem. A* **2008**, *112*, 4360−4366.
(12) Chen, X. J.; Wu, F.; Yan, M.; Shan, X.; Xu, K. Determining Conformational Preference for Molecules by Electron Momentum Spectroscopy. *J. Phys. Conf. Ser.* **2007**, *80*, 012003.
(13) McCarthy, I. E.; Weigold, E. (e,2e) Spectroscopy. *Phys. Rep.* **1976**, *27*, 275−371.
(14) McCarthy, I. E.; Weigold, E. Wavefunction Mapping in Collision Experiments. *Rep. Prog. Phys.* **1988**, *51*, 299−392.
(15) Weigold, E.; McCarthy, I. E. *Electron Momentum Spectroscopy*; Kluwer Academic-Plenum: New York, 1999.
(16) Neudatchin, V. G.; Popov, Y. V.; Smirnov, Y. F. Electron Momentum Spectroscopy of Atoms, Molecules, and Thin Films. *Physics-Uspekhi* **1999**, *42*, 1017−1044.
(17) Lahmam-Bennani, A. Thirty Years of Experimental Electron−Electron (e,2e) Coincidence Studies: Achievements and Perspectives. *J. Electron Spectrosc. Relat. Phenom.* **2002**, *123*, 365−376.
(18) Deleuze, M. S.; Pang, W. N.; Salam, A.; Shang, R. C. Probing Molecular Conformations with Electron Momentum Spectroscopy: The Case of n-Butane. *J. Am. Chem. Soc.* **2001**, *123*, 4049−4061.
(19) Huang, Y. R.; Knippenberg, S.; Hajgató, B.; François, J.-P.; Deng, J. K.; Deleuze, M. S. Imaging Momentum Orbital Densities of Conformationally Versatile Molecules: A Benchmark Theoretical Study of the Molecular and Electronic Structures of Dimethoxymethane. *J. Phys. Chem. A* **2007**, *111*, 5879−5897.
(20) Deleuze, M. S.; Knippenberg, S. Study of the Molecular Structure, Ionization Spectrum, and Electronic Wave Function of 1,3-Butadiene using Electron Momentum Spectroscopy and Benchmark Dyson Orbital Theories. *J. Chem. Phys.* **2006**, *125*, No. 104309.
(21) Ning, C. G.; Huang, Y. R.; Zhang, S. F.; Deng, J. K.; Liu, K.; Luo, Z. H.; Wang, F. Experimental and Theoretical Electron Momentum Spectroscopic Study of the Valence Electronic Structure of Tetrahydrofuran under Pseudorotation. *J. Phys. Chem. A* **2008**, *112*, 11078−11087.
(22) Xue, X. X.; Yan, M.; Wu, F.; Shan, X.; Xu, K. Z.; Chen, X. J. Electron Momentum Spectroscopy of Ethanethiol Complete Valence Shell. *Chin. J. Chem. Phys.* **2008**, *21*, 515−520.

(23) Yan, M.; Shan, X.; Wu, F.; Xia, X.; Wang, K. D.; Xu, K. Z.; Chen, X. J. Electron Momentum Spectroscopy Study on Valence Electronic Structures of Ethylamine. *J. Phys. Chem. A* **2009**, *113*, 507−512.
(24) Morini, F.; Hajgató, B.; Deleuze, M. S.; Ning, C. G.; Deng, J. K. Benchmark Dyson Orbital Study of the Ionization Spectrum and Electron Momentum Distributions of Ethanol in Conformational Equilibrium. *J. Phys. Chem. A* **2008**, *112*, 9083−9096.
(25) Morini, F.; Knippenberg, S.; Deleuze, M. S.; Hajgató, B. Quantum Chemical Study of Conformational Fingerprints in the Photoelectron Spectra and (e,2e) Electron Momentum Distributions of n-Hexane. *J. Phys. Chem. A* **2010**, *114*, 4400−4417.
(26) Shojaei, S. H. R.; Morini, F.; Deleuze, M. S. Photoelectron and Electron Momentum Spectroscopy of Tetrahydrofuran from a Molecular Dynamical Perspective. *J. Phys. Chem. A* **2013**, *117*, 1918−1929.
(27) (a) Haile, J. M. *Molecular Dynamics Simulation*; John Wiley & Sons: New York, 1997. (b) Cramer, C. J. *Essentials of Computational Chemistry*; Wiley: New York, 2004.
(28) Deleuze, M.; Pickup, B. T.; Delhalle, J. Plane wave and orthogonalized plane wave many-body Green's function calculations of photoionization intensities. *Mol. Phys.* **1994**, *83*, 655.
(29) Bultinck, P.; Girones, X.; Carbó-Dorca, R. Molecular Quantum Similarity: Theory and Applications. *Rev. Comput. Chem.* **2005**, *21*, 127−207.
(30) Allan, N. L.; Cooper, D. L. A Momentum-Space Approach to Molecular Similarity. *J. Chem. Inf. Comput. Sci.* **1992**, *32*, 587−590.
(31) Allan, N. L.; Cooper, D. L. Momentum-Space Electron-Densities and Quantum Molecular Similarity. *Mol. Similar. I* **1995**, *173*, 85−111.
(32) Allan, N. L.; Cooper, D. L. Quantum molecular similarity via momentum-space indices. *J. Math. Chem.* **1998**, *23*, 51−60.
(33) Vivas-Reyes, R.; Ariasa, A.; Vandenbussche, J.; Bultinck, P.; Van Alsenoy, C. Quantum similarity of isosteres: coordinate versus momentum space and influence of alignment. *J. Mol. Struct. (THEOCHEM)* **2010**, *943*, 183−188.
(34) See: http://dasher.wustl.edu/ffe/.
(35) Allinger, N. L.; Yuh, Y. H.; Lii, J. H. Molecular Mechanics. The MM3 Force Field for Hydrocarbons. 1. *J. Am. Chem. Soc.* **1989**, *111*, 8551−8566.
(36) Lii, J. H.; Allinger, N. L. Molecular Mechanics. The MM3 Force Field for Hydrocarbons. 2. Vibrational Frequencies and Thermodynamics. *J. Am. Chem. Soc.* **1989**, *111*, 8566−8575.
(37) Lii, J. H.; Allinger, N. L. Molecular Mechanics. The MM3 Force Field for Hydrocarbons. 3. The Van der Waals' Potentials and Crystal Data for Aliphatic and Aromatic Hydrocarbons. *J. Am. Chem. Soc.* **1989**, *111*, 8576−8582.
(38) Nevins, N.; Lii, J.-H.; Allinger, N. L. Molecular Mechanics (MM4) Calculations on Conjugated Hydrocarbons. *J. Comput. Chem.* **1996**, *17*, 695−729.
(39) Gundertofte, K.; Liljefors, T.; Norrby, P.-O.; Petterson, I. A Comparison of Conformational Energies Calculated by Several Molecular Mechanics Methods. *J. Comput. Chem.* **1996**, *17*, 429−449.
(40) Gonzalez, C.; Lim, E. C. A Quantum Chemistry Study of the Van der Waals Dimers of Benzene, Naphthalene, and Anthracene: Crossed (D_{2d}) and Parallel-Displaced (C_{2h}) Dimers of Very Similar Energies in the Linear Polyacenes. *J. Phys. Chem. A* **2000**, *104*, 2953−2957.
(41) Deleuze, M. S.; Leigh, D. A.; Zerbetto, F. How Do Benzylic Amide [2]Catenane Rings Rotate? *J. Am. Chem. Soc.* **1999**, *121*, 2364−2379.
(42) Kwasniewski, S. P.; Claes, L.; François, J. P.; Deleuze, M. S. High Level Theoretical Study of the Structure and Rotational Barriers of *trans*-Stilbene. *J. Chem. Phys.* **2003**, *118*, 7823−7836.
(43) Berendsen, H. J. C.; Postma, J. P. M.; van Gunsteren, W. F.; DiNola, A.; Haak, J. R. Molecular Dynamics with Coupling to an External Bath. *J. Chem. Phys.* **1984**, *81*, 3684−3690.
(44) Beeman, D. Some Multistep Methods for Use in Molecular Dynamics Calculations. *J. Comput. Phys.* **1976**, *20*, 130−139.
(45) Becke, A. D. Density-Functional Thermochemistry. III. The Role of Exact Exchange. *J. Chem. Phys.* **1993**, *98*, 5648−5652.
(46) Lee, C.; Yang, W.; Parr, R. G. Development of the Colle-Salvetti Correlation-Energy Formula into a Functional of the Electron Density. *Phys. Rev. B* **1988**, *37*, 785−789.
(47) Chai, J. D.; Head-Gordon, M. Long-Range Corrected Hybrid Density Functionals with Damped Atom−Atom Dispersion Corrections. *Phys. Chem. Chem. Phys.* **2008**, *10*, 6615−6620.
(48) Dunning, T. H., Jr. Gaussian Basis Sets for use in Correlated Molecular Calculations. I. The Atoms Boron through Neon and Hydrogen. *J. Chem. Phys.* **1989**, *90*, 1007−1023.
(49) Kendall, R. A.; Dunning, T. H., Jr.; Harrison, R. Electron Affinities of the First-Row Atoms Revisited. Systematic Basis Sets and Wave Functions. *J. Chem. Phys.* **1992**, *96*, 6796−6806.
(50) Frisch, M. J.; et al. *Gaussian 09*, revision B.01; Gaussian, Inc.: Wallingford, CT, 2009.
(51) Cederbaum, L. S.; Domcke, W. Theoretical Aspects of Ionization Potentials and Photoelectron Spectroscopy: A Green's Function Approach. *Adv. Chem. Phys.* **1977**, *36*, 205−344.
(52) von Niessen, W.; Schirmer, J.; Cederbaum, L. S. Computational Methods for the One-Particle Green's Function. *Comput. Phys. Rep.* **1984**, *1*, 57−125.
(53) Parr, R. G.; Yang, W. *Density-Functional Theory of Atoms and Molecules*; Oxford University Press: New York, 1989.
(54) Chong, D. P.; Gritsenko, O. V.; Baerends, E. J. Interpretation of the Kohn−Sham Orbital Energies as Approximate Vertical Ionization Potentials. *J. Chem. Phys.* **2002**, *116*, 1760−1772.
(55) Stowasser, R.; Hoffmann, R. What Do the Kohn-Sham Orbitals and Eigenvalues Mean? *J. Am. Chem. Soc.* **1999**, *121*, 3414−3420.
(56) Deleuze, M. S. Valence One-Electron and Shake-Up Ionization Bands of Polycyclic Aromatic Hydrocarbons. II. Azulene, Phenanthrene, Pyrene, Chrysene, Triphenylene, and Perylene. *J. Chem. Phys.* **2002**, *116*, 7012−7026.
(57) Deleuze, M. S. Valence One-Electron and Shake-Up Ionization Bands of Polycyclic Aromatic Hydrocarbons. III. Coronene, 1.2,6.7-Dibenzopyrene, 1.12-Benzoperylene, Anthanthrene. *J. Phys. Chem. A* **2004**, *108*, 9244−9259.
(58) Deleuze, M. S. Valence One-Electron and Shake-Up Ionisation Bands of Polycyclic Aromatic Hydrocarbons. IV. The Dibenzanthracene Species. *Chem. Phys.* **2006**, *329*, 22−38.
(59) Cederbaum, L. S.; Schirmer, J.; Domcke, W.; von Niessen, W. Correlation Effects in the Ionization of Molecules: Breakdown of the Molecular Orbital Picture. *Adv. Chem. Phys.* **1986**, *65*, 115−159.
(60) Bawagan, A. D. O. *HEMS program, Evaluation of Wave Functions by Electron Momentum Spectroscopy*; Ph.D. Thesis; University of British Columbia, 1987. The HEMS (now known as MOMAP) program has been extensively revised and extended at UBC by Cann, , N. M.; Cooper, , G..
(61) Ning, C. G.; Ren, X. G.; Deng, J. K.; Su, G. L.; Zhang, S. F.; Knippenberg, S.; Deleuze, M. S. Probing Dyson Orbitals with Green's Function Theory and Electron Momentum Spectroscopy. *Chem. Phys. Lett.* **2006**, *421*, 52−57.
(62) Ning, C. G.; Hajgató, B.; Huang, Y. R.; Zhang, S. F.; Liu, K.; Luo, Z. H.; Knippenberg, S.; Deng, J. K.; Deleuze, M. S. High Resolution Electron Momentum Spectroscopy of the Valence Orbitals of Water. *Chem. Phys.* **2008**, *343*, 19−30.
(63) Duffy, P.; Cassida, M. E.; Brion, C. E.; Chong, D. P. Assessment of Gaussian-Weighted Angular Resolution Functions in the Comparison of Quantum Mechanically Calculated Electron Momentum Distributions with Experiment. *Chem. Phys.* **1992**, *159*, 347−363.
(64) See: http://getdata-graph-digitizer.com/.
(65) Staroverov, V. N.; Davidson, E. R. *Ab initio* Compton Maps of Small Molecules. *Mol. Phys.* **2001**, *99*, 175−186.
(66) Hart, J. R.; Thakkar, A. J. Moments of the Electron Momentum Density: Requirements for ab initio and Density Functional Theory Calculations. *Int. J. Quantum Chem.* **2005**, *102*, 673−683.
(67) Miguel, B.; de la Vega, J. M. G. Influence of Electronic Correlation in Monoelectronic Density in p-Space. *Theor. Chem. Acc.* **2007**, *118*, 723−732.

(68) Ragot, S. Exact Kohn-Sham Versus Hartree-Fock in Momentum Space: Examples of Two-Fermion Systems. *J. Chem. Phys.* **2006**, *125*, 014106.
(69) Gritsenko, O. V.; Braida, B.; Baerends, E. J. Physical Interpretation and Evaluation of the Kohn-Sham and Dyson Components of the Epsilon-I Relations Between the Kohn-Sham Orbital Energies and the Ionization Potentials. *J. Chem. Phys.* **2003**, *119*, 1937−1950.
(70) Thakkar, A. J.; Sharma, B. S. A Fresh Look at the Computation of Spherically Averaged Electron Momentum Densities for Wave Functions Built from Gaussian-type Functions. *Int. J. Quantum Chem.* **2001**, *85*, 258−262.
(71) White, R. M.; Carlson, T. A.; Spears, D. P. Angular Distribution of the Photoelectron Spectra for Ethylene, Propylene, Butene and Butadiene. *J. Electron Spectrosc. Relat. Phenom.* **1974**, *3*, 59−70.